Characterization of the Three-Dimensional Solution Structure of Human Profilin: ^{1}H, ^{13}C, and ^{15}N NMR Assignments and Global Folding Pattern

William J. Metzler,* Keith L. Constantine, Mark S. Friedrichs, Aneka J. Bell, Eileen G. Ernst, Thomas B. Lavoie, and Luciano Mueller

Departments of Macromolecular NMR and Macromolecular Biochemistry, Bristol-Myers Squibb Pharmaceutical Research Institute, Princeton, New Jersey 08543-4000

Received July 23, 1993; Revised Manuscript Received September 28, 1993●

ABSTRACT: Human profilin is a 15-kDa protein that plays a major role in the signaling pathway leading to cytoskeletal rearrangement. Essentially complete assignment of the ^{1}H, ^{13}C, and ^{15}N resonances of human profilin have been made by analysis of multidimensional, double- and triple-resonance nuclear magnetic resonance (NMR) experiments. The deviation of the $^{13}C\alpha$ and $^{13}C\beta$ chemical shifts from their respective random coil values were analyzed and correlate well with the secondary structure determined from the NMR data. Twenty structures of human profilin were refined in the program X-PLOR using a total of 1186 experimentally derived conformational restraints. The structures converged to a root mean squared distance deviation of 1.5 Å for the backbone atoms. The resultant conformational ensemble indicates that human profilin is an α/β protein comprised of a seven-stranded, antiparallel β-sheet and three helices. The secondary structure elements for human profilin are quite similar to those found in *Acanthamoeba* profilin I [Archer, S. J., Vinson, V. K., Pollard, T. D., & Torchia, D. A. (1993), *Biochemistry* 32, 6680–6687], suggesting that the three-dimensional structure of *Acanthamoeba* profilin I should be analogous to that determined here for human profilin. The structure determination of human profilin has facilitated the sequence alignment of lower eukaryotic and human profilins and provides a framework upon which the various functionalities of profilin can be explored. At least one element of the actin-binding region of human profilin is an α-helix. Two mechanisms by which phosphatidylinositol 4,5-bisphosphate can interfere with actin-binding by human profilin are proposed.

Profilin is a small cytoplasmic protein that appears to be essential for the cytoskeletal rearrangement of cells. Profilin interacts reversibly with actin and phophoinositides and is thus believed to regulate actin filament assembly in response to cell surface-mediated signaling events. At high profilin-to-actin ratios, profilin sequesters actin monomers in vitro thereby preventing actin filament formation (Haarer & Brown, 1990; Goldschmidt-Clermont & Janmey, 1991). The cellular concentration of profilin is insufficient to bind all of the actin (Goldschmidt-Clermont & Janmey, 1991); however, profilin may regulate actin filamentation by modulation of the equilibrium concentration of monomeric actin in vivo. Alternatively, profilin can catalyze the exchange of ADP for ATP on monomeric actin, a rate-limiting step in actin polymerization, suggesting that profilin also has the ability to promote actin polymerization (Mockrin & Korn, 1980; Goldschmidt-Clermont et al., 1991b).

Formation of the profilin–actin complex is regulated, at least in part, by the interaction of profilin with the membrane phospholipid bilayer. It has been demonstrated that profilin binds tightly and specifically to phosphatidylinositol 4,5-bisphosphate (PIP_2)[1] in vitro, resulting in a dissociation of the profilin–actin complex (Lassing & Lindberg, 1985). Concomitantly, profilin masks PIP_2 from the hydrolytic action of phospholipase C-γ1 (Goldschmidt-Clermont et al., 1990). Phosphorylation enables phospholipase C-γ1 to overcome profilin's inhibitory effects on the cleavage of PIP_2 (Goldschmidt-Clermont et al., 1991a), causing the profilin–PIP_2 complex to dissociate and allowing profilin to interact with actin. All of the above observations suggest that profilin provides a link between the phosphatidylinositol cycle (a major signal transduction pathway) and the actin cytoskeleton.

The primary structures of profilins from many species are known. Profilins range in size from 123 to 139 amino acids; the profilins from lower eukaryotes have approximately 30% homology to those of mammals. While this degree of homology would normally be sufficient for sequence alignment purposes, extremely divergent regions in the middle of the sequences, and the deletion of 10–20 residues in the sequence of lower eukaryotic profilins, complicate the alignment process. Several sequence alignments have been proposed (Takagi et al., 1990; Binette et al., 1990; Kwiatkowski & Bruns, 1988; Pollard & Rim, 1991). The difficulties encountered in aligning the amino acid sequences of profilin have hindered attempts to gain insight into the functions of profilin through analysis of sequence homologies.

The multiple roles that profilins may play in the cell have made it the target of intense biological research. Knowledge of the three-dimensional structure of profilins will facilitate their sequence alignment and, ultimately, will afford detailed information concerning structure/function relationships. Because profilins are relatively small proteins with molecular weights around 15 000, they are well suited for study by nuclear magnetic resonance (NMR) spectroscopy. We describe here the ^{1}H, ^{15}N, and ^{13}C NMR assignments for human profilin

* To whom correspondence should be addressed.

● Abstract published in *Advance ACS Abstracts*, November 15, 1993.

[1] Abbreviations: PIP_2, phosphatidylinositol 4,5-bisphosphate; NMR, nuclear magnetic resonance; FID, free induction decay; HMQC, heteronuclear multiple-quantum coherence; HSQC, heteronuclear single-quantum coherence; NOE, nuclear Overhauser effect; NOESY, nuclear Overhauser effect spectroscopy; TOCSY, total correlation spectroscopy; 2D, two dimensional; 3D, three dimensional; 4D, four dimensional; rmsd, root mean squared deviation.

0006-2960/93/0432-13818$04.00/0

and characterize its three-dimensional conformation in solution.

EXPERIMENTAL PROCEDURES

Sample Preparation. Recombinant human profilin was prepared by subcloning the cDNA for the human profilin gene (gift from D. J. Kwiatkowski, Massachusetts General Hospital) into the pGTL-1 expression vector (T. B. Lavoie, unpublished). *Escherichia coli* were grown in M9 minimal medium supplemented with minerals and vitamin B12. Human profilin samples were uniformly enriched with ^{15}N and/or ^{13}C by providing $^{15}NH_4Cl$ (Isotec Inc., Miamisburg, OH) as the sole nitrogen source and [$^{13}C_6$]-D-glucose/sodium [$^{13}C_2$]acetate (Isotec Inc, Miamisburg, OH) as the sole carbon sources. The protein was purified and assayed as described (Kaiser et al., 1989; T. B. Lavoie, unpublished). Yields of profilin were approximately 15–25 mg of purified protein per liter cell growth.

The buffer for all NMR experiments contained the following: 10 mM phosphate, 25 mM KCl, 20 mM β-mercaptoethanol, and 1 mM EDTA, pH 6.4. The buffer was made in either 90% H_2O/10% ^2H_2O or 100% ^2H_2O (99.996% ^2H_2O (MSD Isotopes, Montreal, Canada). Samples of profilin were prepared by dialyzing 30 mg of profilin (~1 mg/mL) against 10 L of buffer and concentrating the solution to 2.0 mM in a final volume of 0.6 mL.

NMR Spectroscopy. All NMR experiments were performed on a Varian Unity 600 spectrometer equipped with a ^1H–^{13}C–^{15}N triple-tuned probe and a waveform generator. Unless otherwise noted, the following are the standard parameters with which spectra were acquired: carrier frequencies were set at 4.85 ppm (^1H), 119.5 ppm (^{15}N), 45.2 ppm (^{13}C aliphatic), and 127.5 ppm (^{13}C aromatic); spectral widths were 8000 Hz (^1H), 2000 Hz (^{15}N), and 3000 Hz (^{13}C); the ^1H acquisition time was 0.128 s. Multidimensional NMR spectra were recorded in the phase-sensitive mode with a States-TPPI type acquisition scheme (Marion et al., 1989a) for all nonacquisition dimensions. For experiments in which only the amide protons were of interest in the acquisition dimension, the spectral region upfield of the water resonance was discarded. All spectra were recorded at 20 °C.

Spectra were processed using a version of FELIX (Hare Research, Bothell, WA) modified to incorporate complex linear prediction (Zhu & Bax, 1990; M. Friedrichs, unpublished). In some cases, "mirror image" linear prediction was performed after extending the signal into the negative time domain (Zhu & Bax, 1990). For spectra recorded with samples in H_2O, low-frequency deconvolution was applied to the acquisition FIDs prior to transformation in order to reduce the size of the residual H_2O (Marion et al., 1989b).

2D HSQC ^{15}N–^1H correlation spectra (Bodenhausen & Ruben, 1980) were acquired by collecting a total of 256 complex FIDs in t_1 by hypercomplex acquisition (Mueller & Ernst, 1978; States et al., 1982), with eight scans signal-averaged per FID. Amide hydrogen exchange rates were determined by passing profilin over a G25-Sepharose column which had been equilibrated with ^2H_2O buffer and acquiring a series of 2D HSQC ^{15}N–^1H correlation spectra (128 t_1 FIDs) at 1, 2, 4, 8, 24, and 96 h after the exchange was initiated.

3D HNCACB (Wittekind & Mueller, 1993) and 3D CBCA(CO)HN (Grzesiek & Bax, 1992) spectra were acquired with a ^{13}C spectral width of 9000 Hz (F_1) by collecting 38 complex FIDs in F_1 and 32 complex FIDs in F_2 with 32 scans per FID. An additional 32 complex points were obtained in F_2 by using linear prediction. The data were processed into a 256 × 128 × 512 real matrices.

The 3D HBHA(CO)HN spectrum (Grzesiek & Bax, 1992) was acquired by collecting 32 complex FIDs in F_1 and 30 complex FIDs in F_2 with 32 scans per FID. The number of data points was increased to 64 in F_1 and F_2 by using linear prediction. The data were processed into a 256 × 128 × 512 real matrix.

The 3D HNHA(gly) spectrum (Wittekind et al., 1993) was acquired by collecting 22 complex FIDs in F_1 and 32 complex FIDs in F_2 with 64 scans per FID. An additional 32 complex points were obtained in F_2 by using linear prediction. The data were processed into a 128 × 128 × 512 real matrix.

4D HNCAHA and HN(CO)CAHA spectra (Kay et al., 1992; Olejniczak et al., 1992) were acquired by collecting 10 complex FIDs in F_1, eight complex FIDs in F_2, and 20 complex FIDs in F_3, with 16 scans per FID. The number of data points in each nonacquisition dimension was increased to 32 by using linear prediction. The data were processed into 64 × 64 × 64 × 256 real matrices.

3D HCCH-COSY and HCCH-TOCSY spectra were obtained using the published pulse sequences (Bax et al., 1990) modified to allow eight-step phase cycling per F_1(^1H)–F_2-(^{13}C) point (Constantine et al., 1993). The spectral width for ^1H in both F_1 and F_3 was 6000 Hz. A total of 176 complex FIDs in F_1 and 32 complex FIDs in F_2 were acquired, with eight scans per FID. Carbonyl decoupling during t_2 was performed with a frequency-shifted cosine-modulated SEDUCE pulse scheme (McCoy & Mueller, 1992). The DIPSI-3 isotropic mixing sequence (Shaka et al., 1988) with a mixing time of 24 ms was used for the HCCH-TOCSY experiment. The number of data points in F_2 was doubled with linear prediction. The data were processed into 512 × 128 × 512 matrices.

3D ^{15}N-edited NOESY-HSQC (Marion et al., 1989a,b; Zuiderweg & Fesik, 1990; Mueller et al., 1992) and ^{13}C-edited NOESY-HMQC spectra (Ikura et al., 1990; Zuiderweg et al., 1990) were obtained by collecting 128 complex FIDs in F_1 and 32 complex FIDs in F_2 with eight scans per FID. An additional 32 complex points were obtained in F_2 by using linear prediction. The data were processed into a 512 × 128 × 512 real matrix. The ^{13}C-edited NOESY-HMQC spectra were collected with mix times of 30 and 60 ms, and the ^{15}N-edited NOESY-HSQC was recorded with a mixing time of 100 ms.

Derivation of Structural Restraints. Three types of restraints for the structure calculations were derived from the NMR data: interproton distance restraints, torsion angle restraints, and hydrogen bond restraints.

A total of 1005 physically significant distance restraints were derived from the cross-peak intensities of the ^{15}N-edited NOESY-HSQC and ^{13}C-edited NOESY-HMQC spectra. These restraints included: 153 intraresidue restraints, 373 sequential restraints, 208 medium-range restraints ($|i-j| < 4$), and 271 long-range restraints ($|i-j| > 4$). Each interresidue NOE was converted into an interproton distance by normalizing its integrated cross-peak volume against a calibrated volume. For the ^{13}C aromatic spectrum, intraresidue Trp ring NOEs were used as calibrations. For the remaining spectra, backbone–backbone NOEs within the identified β-sheet regions were used with reference to the typical distance ranges for these interactions (Wüthrich, 1986). For example, the average volume of Hα–Hα NOEs between β-strands was used to establish a calibration standard for very strong NOEs in the aliphatic ^{13}C-edited 3D NOESY-HMQC spectrum.

The distance for this interaction is 2.3 Å in regular antiparallel β-sheets (Wüthrich, 1986). The NOEs were then classified as very strong, strong, medium, or weak, corresponding to interproton upper distance bounds of less than 2.5, 3.0, 4.0, and 5.0 Å, respectively. In order to establish calibration volumes for the 3.0, 4.0, and 5.0 Å bins, the relation $V_a = V_b(r_b/r_a)^6$ was used. Since spin diffusion is expected to make greater contributions to relatively weak NOE cross-peaks, an additional 20–30% was added to the resulting calibration volumes V_a for the longer distance bins. Restraint ranges were generated by setting the lower bounds equal to the sum of the van der Waals radii (1.8 Å) and by correcting upper bounds involving equivalent and/or nonstereospecifically assigned groups for use as $(\Sigma r^{-6})^{-1/6}$ effective distances (Constantine et al., 1992).

A total of 85 torsion angle restraints for the backbone torsion angle Φ were derived from the value of $^3J_{HN\alpha}$ measured in the HMQC-J (Kay & Bax, 1989) and *J*-modulated [^{15}N,^{1}H]-COSY experiments (64-step phase cycle; Billeter et al., 1992); the latter were recorded with variable delays of 15, 25, 40, 60, 80, and 100 ms. Torsion angle restraint ranges for Φ were set to −120° ± 40° (for $^3J_{HN\alpha} > 8.5$ Hz), −120° ± 50° (for 8.5 Hz > $^3J_{HN\alpha} > 8.0$ Hz), and −60° ± 40° (for $^3J_{HN\alpha} < 5.0$ Hz and when the NOE data indicated the presence of a helix). For a restraint to be included, the derived value of Φ must have been consistent with the $^3J_{HN\alpha}$ and NOE data.

Hydrogen bond restraints were derived from an analysis of the amide proton exchange rates. Restraints were included only if the amide hydrogen was shown to have a reduced exchange rate and the initial structure calculations provided unambiguous identification of the hydrogen bond acceptor. In total, 96 restraints defining 48 hydrogen bonds were included; for each hydrogen bond, the HN–O and the N–O distances were restrained to be 2.0 ± 0.4 and 3.0 ± 0.4 Å, respectively.

Structure Calculations. Structure calculations were performed with the program X-PLOR on a CRAY YMP2 supercomputer. An initial set of 20 structures was generated by selecting random values for the Φ and Ψ torsion angles. These random structures were then refined using only unambiguous restraints (i.e., those restraints which are defined uniquely by the chemical shift information) to produce a set of preliminary structures. Examination of these structures allowed many of the ambiguities in the assignment of NOE cross-peaks to be resolved and lead to the identification of many of the hydrogen bond acceptors of the slowly exchanging amide hydrogens. These additional restraints were then used to refine further the preliminary structures, and the process was repeated. The protocol used to refine the structures in X-PLOR has been described in detail (Nilges et al., 1988; Brunger, 1992; Metzler et al., 1992). Briefly, the procedure involves an initial Powell minimization of the random structures to remove bad steric interactions, followed by extensive dynamic simulated annealing and a final round of Powell minimization. During the initial stage of dynamic simulated annealing, restraints are weighted so that the penalty assessed to the largest violations is reduced, and the repulsive interactions are greatly attenuated. The reduced penalties in effect allow the local structure to form before the global structure and helps prevent "knotting" of the structure. The repulsive potential is then increased gradually, as is the penalty assessed to the largest restraint violations. A final round of annealing ensures that the structure is in a local minimum with respect to all potential terms applied (repulsion, bonds, angles, impropers, NOE, and torsion angle restraints).

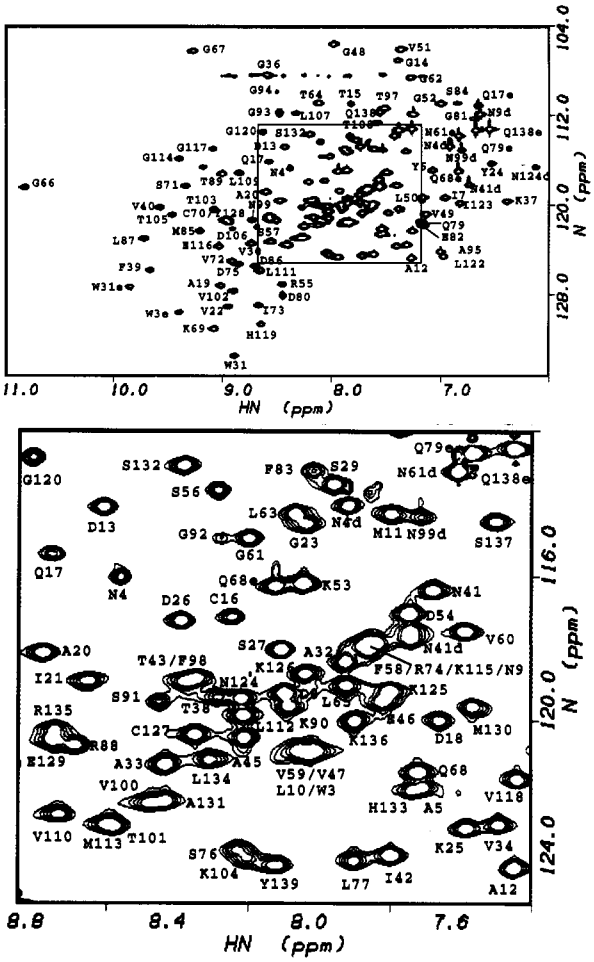

FIGURE 1: ^{1}H–^{15}N HSQC spectrum of uniformly ^{15}N-labeled human profilin. Cross-peak assignments are indicated with the one-letter amino acid code and residue number. The cross-peaks in the box in the full HSQC spectrum (top) is expanded in the bottom panel.

Refined structures were analyzed for best fit to the NMR restraints and the overall energy. Examination of the best 10 structures indicated that the overall three-dimensional fold of profilin is well-determined by the current NMR data set.

RESULTS

Sequence-Specific Resonance Assignments. Figure 1 shows the 2D ^{15}N–^{1}H HSQC spectrum of uniformly ^{15}N-labeled profilin. Also shown in this figure are the assignments of the cross-peaks that were ultimately determined as described below. This spectrum was collected with an increased spectral width (4000 Hz) to ensure that cross-peaks were not folded in the ^{15}N dimension. The cross-peaks are well dispersed in both dimensions. The large chemical shift dispersion and the presence of a single set of resonances for each amino acid indicate that the protein is a single species with a stable tertiary fold.

Sequential resonance assignments were made through analysis of five experiments: the 3D HNCACB and CBCA-(CO)HN experiments, the 4D HNCAHA and HN(CO)-CAHA experiments, and the 3D HNHA(gly) experiment. The first step in making assignments was to build spin systems consisting of the ^{1}HN(i), ^{15}N(i), ^{13}Cα(i), ^{13}Cβ(i), ^{1}Hα(i), ^{13}Cα-(i−1), ^{13}Cβ(i−1), and ^{1}Hα(i−1) resonances. The HNCACB experiment, which is analogous to the CBCAHN experiment (Greziek & Bax, 1992), afforded the majority of these spin system identifications. In this experiment, the intraresidue and sequential Cβ and Cα resonances are correlated to the

amide proton of the proceeding residue. The Cβ and Cα resonances are easily distinguished in this spectrum, as their cross-peaks are of opposite sign. The intraresidue and sequential resonances were distinguished on the basis of peak intensity and by comparison with data from the CBCA(CO)-HN experiment. The spin systems were extended to the Hα-(i) and Hα(i–1) resonances with the two 4D experiments. These experiments also confirmed the Cα identifications. Finally, the 3D HNHA[gly] experiment provided the Hα(i) and Hα(i–1) identifications for glycine residues, which often were not observable in the above 4D spectra.

Spin systems were linked by matching the ^{13}Cα(i),^{13}Cβ(i), and ^{1}Hα(i) chemical shifts of an HN/N pair with the ^{13}Cα-(i–1), ^{13}Cβ(i–1), and ^{1}Hα(i–1) chemical shifts of another HN/N pair. In this way, numerous stretches of sequentially aligned spin systems were generated. To obtain sequence specific assignments, "marker" spin systems were identified. These markers included threonine and serine residues, which were easily identified by their Cβ resonances being downfield of their Cα resonances; alanine residues, which were identified by the characteristic chemical shift of their Cβ resonances; and glycine residues, which were identified by the characteristic chemical shift of their Cα resonances and the absence of a Cβ resonance. The identities of the remaining spin systems were restricted to a subset of possible residue types by analyzing their Cα/Cβ chemical shifts and the probabilities that these chemical shifts were characteristic of a particular amino acid type. At this point, it was straightforward to assign specific residues to each of the stretches of connected spin systems. Figure 2 shows an example wherein connectivities are made from Thr 96 through Lys 125. In total, assignments were obtained for all residues except the N-terminal alanine and glycine residues.

Aliphatic side chain ^{1}H and ^{13}C resonances were assigned primarily by analyzing the 3D HCCH-COSY and HCCH-TOCSY spectra by methods previously described (Clore et al., 1990; Constantine et al., 1993). The side chain assignments served to confirm the sequential backbone assignments described above and provided support for the use of chemical shifts in grouping spin systems into subclasses of amino acid types.

Aromatic side chain ^{1}H and ^{13}C resonances were assigned by analyzing the HCCH-TOCSY and ^{13}C-edited NOESY-HMQC spectra that were optimized for aromatic carbon resonances. Each aromatic side chain resonance was classified to amino acid type with the TOCSY spectrum and then assigned to its specific location in the profilin amino acid sequence through detection of NOEs from the aromatic side chain to the intraresidue ^{1}Hβs and ^{1}Hαs. Aromatic side chain ^{1}H and ^{15}N resonances for tryptophans were assigned by detection of NOEs to the other ring protons in the ^{15}N-edited NOESY-HSQC and ^{13}C-edited NOESY-HMQC spectra.

Side chain ^{1}H and ^{15}N for glutamines and asparagines were assigned by identifying NOEs between the side chain amide protons and ^{1}Hβ and ^{1}Hγ protons in the ^{15}N-edited NOESY-HSQC. Cross-peaks between these resonances were also observed in the HNCACB spectrum (Wittekind & Mueller, 1993).

The ^{1}H, ^{15}N, and ^{13}C assignments are summarized in Table I. Assignments were made for 98% of the ^{1}H resonances. Rapid exchange of the amide hydrogens for the N-terminal ammonium and Gly 2 precluded the assignment of these residues, although the Hαs of Gly 2 were tentatively identified by observation of sequential NOEs to the Trp 3 amide proton. Assignments of several of the lysine and arginine side chains were ambiguous due to spectral overlap in the 3D spectra. In addition, assignments for the methyl resonances for several of the methionines have not yet been obtained.

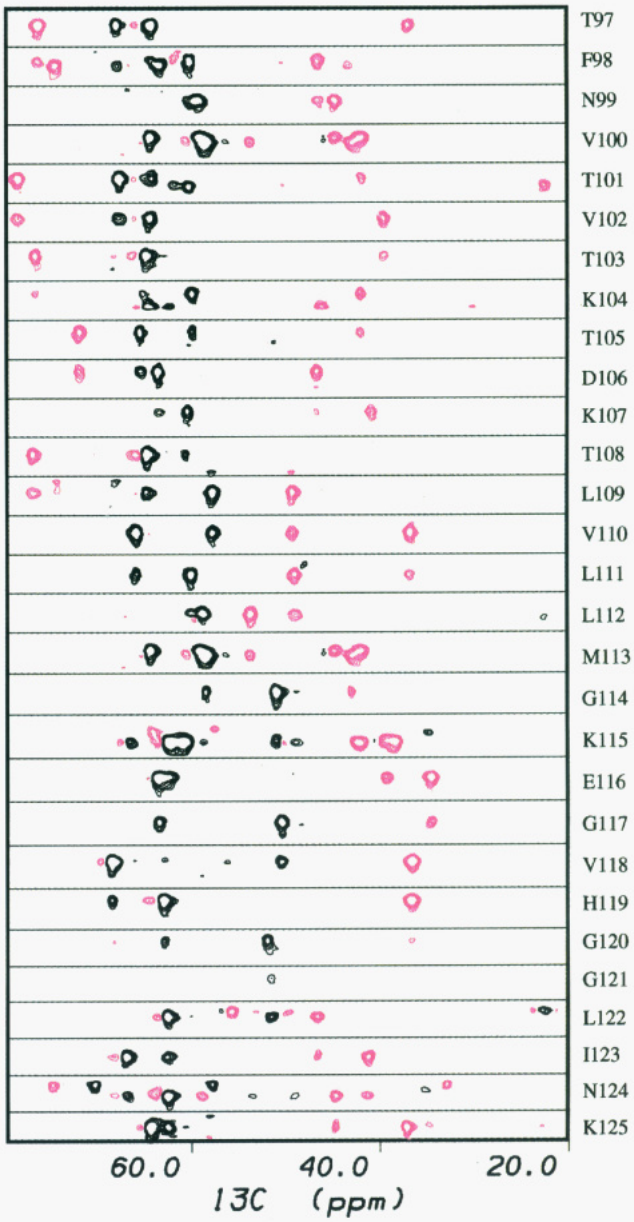

FIGURE 2: Strip plot of selected regions of the 3D HNCACB spectrum of human profilin illustrating the sequential resonance assignments made for residues 97–125. Each horizontal strip corresponds to the amino acid shown on the right axis. The strips are centered around the amide ^{1}H chemical shift in the plane of its amide ^{15}N chemical shift. Cα (black) and Cβ (red) cross-peaks to the amide hydrogen were used to step sequentially in the N-terminal direction from residue i to residue i–1.

Secondary Structure Analysis. After completion of the resonance assignments, the ^{15}N-edited and ^{13}C-edited spectra were analyzed for the presence of secondary structural elements. Figure 3 summarizes the data obtained for the short- and medium-range NOEs, $^{3}J_{HN\alpha}$ coupling constants, and slowly exchanging amide hydrogens.

Qualitative analysis of sequential and medium-range NOES revealed stretches of d_{NN}, $d_{NN(i,i+2)}$, $d_{\alpha b(i,i+3)}$, $d_{\alpha N(i,i+3)}$, and $d_{\alpha N(i,i+4)}$ NOEs from residues 3 through 14 and from residues 122 through 139, suggesting the presence of helices at the N- and C-termini of profilin. This notion is supported by the detection of small values for the $^{3}J_{HN\alpha}$ coupling constants for these residues as well as by the presence of slowly exchanging

Table I: ^{1}H, ^{15}N, and ^{13}C Resonance Assignments for Human Profilin

ALA	N	HN	CA	HA	CB	HB*
A1						
A5	122.6	7.70	54.8	4.09	17.7	1.16
A12	124.8	7.45	56.0	4.06	19.0	1.53
A19	127.4	9.19	51.8	5.55	23.7	1.41
A20	118.9	8.78	51.8	5.13	24.1	1.28
A32	119.3	7.92	52.7	4.61	23.2	1.48
A33	122.0	8.43	51.7	5.20	22.3	1.46
A45	121.4	8.21	55.8	4.08	18.1	1.36
A95	124.3	7.18	51.0	4.49	17.6	1.49
A131	123.0	8.45	55.6	3.77	17.6	1.38

ARG	N	HN	CA	HA	CB	HB1	HB2	CG	HG1	HG2	CD	HD1	HD2
R55	127.2	8.63	52.5	3.86	28.0	2.10	1.52		1.09	1.09	41.9	3.08	2.92
R74	118.7	7.85	56.2	4.65	33.8	1.82	1.82	26.9	1.58	1.43	42.9	3.21	3.08
R88	121.4	8.69	54.8	5.43	34.3	1.76	1.68	27.4	1.85	1.52	43.7	3.12	3.12
R135	121.0	8.75	59.9	4.41	29.6	1.88	1.88	27.4	1.61	1.56	43.1	3.11	2.96
R136	120.7	7.90	58.9	4.16	30.2	1.98	1.98	28.4	1.89	1.67	43.4	3.26	3.19

ASN	N	HN	CA	HA	CB	HB1	HB2	ND2	HD21	HD22
N4	116.8	8.56	56.6	4.29	37.7	2.90	2.82	114.7	7.91	7.09
N9	118.5	7.76	56.9	4.36	38.9	2.87	2.68	112.0	7.44	6.82
N41	117.2	7.68	52.8	4.85	39.1	2.94	2.79	118.3	7.74	6.91
N61	115.8	8.19	53.9	4.80	40.2	2.85	2.67	113.9	7.60	7.07
N99	121.4	8.90	54.7	5.25	40.3	3.11	2.48	115.1	7.71	6.99
N124	120.1	8.24	57.6	4.30	40.0	2.85	2.62	116.6	9.36	6.30

ASP	N	HN	CA	HA	CB	HB1	HB2
D8	120.2	8.10	57.7	4.22	39.7	2.71	2.60
D13	114.8	8.59	54.2	4.47	40.1	3.18	2.68
D18	120.7	7.66	53.4	4.69	44.4	2.12	1.81
D26	118.0	8.39	56.6	4.15	40.1	2.78	2.67
D54	117.9	7.74	53.8	4.50	40.1	2.78	2.52
D75	125.3	9.03	53.7	5.03	42.8	3.06	2.34
D80	128.2	8.63	55.9	3.87	41.0	2.52	2.52
D86	125.6	8.89	53.1	5.80	42.3	3.16	2.41
D106	122.2	9.08	59.0	4.39	41.9	2.57	2.34

CYS	N	HN	CA	HA	CB	HB1	HB2
C16	117.9	8.24	59.4	5.08	30.7	3.05	2.72
C70	121.4	9.16	58.2	5.18	33.3	2.57	2.43
C127	121.2	8.35	62.3	3.81	26.5	3.02	2.92

GLN	N	HN	CA	HA	CB	HB1	HB2	CG	HG1	HG2	NE2	HE21	HE22
Q17	116.2	8.77	53.7	4.69	30.7	2.00	1.51	38.0	1.40	1.40	111.1	6.82	
Q68	122.2	7.72	54.0	4.36	29.3	2.40	2.10	37.0	2.14	2.14	117.0	8.11	7.02
Q79	122.0	7.34	55.9	4.23	30.1	2.07	1.98	33.9	2.26	2.26	113.3	7.58	6.86
Q138	111.9	7.74	58.0	3.96	25.5	2.19	2.19	34.7	2.20	2.20	113.1	7.45	6.75

GLU	N	HN	CA	HA	CB	HB1	HB2	CG	HG1	HG2
E46	120.1	7.82	59.4	3.99	33.8	1.79	1.69			
E82	121.6	7.36	58.0	4.42	32.1	2.07	1.82	36.5	2.10	2.10
E116	123.9	9.20	58.4	4.13	29.8	2.21	2.02		2.29	2.29
E129	121.3	8.75	59.9	3.99	29.3	2.20	2.08	37.1	2.61	2.36

GLY	N	HN	CA	HA1	HA2
G2			45.9	3.79	3.79
G14	107.1	7.57	46.7	4.18	4.18
G23	115.4	8.04	45.7	3.66	2.99
G36	108.3	8.77	46.2	3.99	3.77
G48	112.1	8.16	46.7	3.75	3.75
G52	111.1	7.18	45.7	4.09	3.95
G62	108.8	7.46	45.4	4.42	3.97
G66	118.5	10.98	46.5	3.87	3.40
G67	106.3	9.45	44.8	4.25	3.36
G81	12.5	6.88	45.3	4.12	3.62
G93	112.2	8.88	46.6	3.87	3.87
G94	109.9	8.68	45.3	3.95	3.67
G114	115.9	9.58	46.3	4.72	4.01
G117	115.1	9.26	45.7	4.15	3.72
G120	113.5	8.81	47.3	3.89	3.63
G121	113.3	9.73	46.9	3.93	3.93

HIS	N	HN	CA	HA	CB	HB1	HB2
H119	130.6	8.82	58.4	4.25	32.1	3.28	3.12
H133	122.7	7.73	59.8	4.31	30.0	3.48	3.28

ILE	N	HN	CA	HA	CB	HB	CG1	HG11	HG12	CG2	MG2	CD	MD
I7	119.3	7.14	62.0	3.64	34.5	2.44	28.4	1.83	1.18	19.1	0.82	8.6	0.60
I21	119.7	8.65	60.6	4.69	41.2	1.45	28.6	1.60	1.60	17.7	0.39	14.9	1.02
I42	124.5	7.79	63.2	4.21	38.4	1.58	31.0	1.89	1.07	17.9	0.72	15.8	0.58
I73	129.1	8.85	61.8	4.12	38.0	1.58	27.8	1.32	1.11	17.5	0.91	11.8	0.65
I123	119.9	7.00	62.2	3.57	36.4	2.13	27.6	1.55	1.29	18.7	0.88	12.9	0.80

Table I (Continued)

LEU	N	HN	CA	HA	CB	HB1	HB2	CG	HG	CD1	MD1	CD2	MD2
L10	121.7	8.03	57.9	4.08	42.5	2.06	2.06	26.9	2.00	23.3	0.96	25.6	0.86
L50	119.4	7.35	58.9	3.73	42.5	2.05	1.06	26.8	1.68	24.8	0.59	26.0	0.59
L63	115.1	8.07	54.3	4.66	42.9	1.66	1.66	25.9	1.04	24.2	0.33	27.1	0.10
L65	119.7	7.92	53.3	4.29	45.3	1.64	0.88	26.0	1.30	24.3	0.63	27.1	0.63
L77	124.8	7.91	57.8	3.67	43.8	1.64	1.33	27.0	1.53	24.9	0.63	26.5	0.63
L78	123.5	7.59	52.9	4.48	40.7	1.76	1.64	29.5	1.56	25.9	0.82	22.0	0.66
L87	123.2	9.90	54.3	5.34	47.1	1.75	1.35	28.1	1.44	28.1	0.66	28.1	0.66
L109	117.2	9.04	55.3	5.14	44.3	1.34	0.82	26.7	1.38	27.3	0.44	23.2	0.28
L111	125.9	8.83	55.6	5.09	44.3	0.48	0.48	29.2	1.16	27.2	0.33	29.2	0.04
L112	120.7	8.21	54.1	5.20	49.0	1.82	1.44	27.8	1.73	27.1	1.23	25.6	1.20
L122	124.7	7.15	58.0	4.18	41.9	1.75	1.75	27.5	1.59	24.4	1.00	25.2	0.90
L134	121.8	8.30	59.1	3.97	41.4	1.97	1.36	28.0	1.68	26.3	0.67	23.4	0.67

LYS	N	HN	CA	HA	CB	HB1	HB2	CG	HG1	HG2	CD	HD1	HD2	CE	HE1	HE2
K25	123.8	7.59	55.9	3.98	32.4	1.52	1.46	25.3	0.81	0.81	22.0	1.17	1.17	41.8	2.88	2.88
K37	119.7	6.57	53.2	4.71	27.9	1.85	1.85		1.27	1.20		1.56	1.44			
K53	117.0	8.04	57.9	3.96	33.2	1.74	1.74	25.1	1.44	1.44	29.2	1.65	1.65	42.1	2.94	2.94
K69	131.3	9.25	58.2	4.30	32.5	1.03	1.03	25.6	1.53	1.37	29.1	1.81	1.62	41.7	2.91	2.91
K90	120.4	8.08	55.5	4.50	34.0	1.70	1.43	25.6	1.29	1.29	29.5	1.56	1.56	42.1	2.80	2.80
K104	124.7	8.20	55.1	5.09	37.4	1.68	1.14	23.9	1.52	0.95	30.0	1.27	1.04	41.0	2.73	2.60
K107	111.9	8.50	55.6	4.04	36.4	1.95	1.95	26.0	1.39	1.24	29.2	1.83	1.65	42.1	3.00	3.00
K115	118.7	7.84	57.5	4.10	34.3	1.98	1.68	28.2	1.14	1.03	29.5	1.68	1.59	42.0	2.81	2.61
K125	120.0	7.81	59.5	4.01	32.6	1.94	1.94		1.53	1.53	29.6	2.20	2.07	37.0	2.63	2.36
K126	119.5	8.04	59.7	4.04	33.5	1.76	1.68	25.1	1.44	1.44	29.1	1.66	1.66	41.9	2.95	2.95

MET	N	HN	CA	HA	CB	HB1	HB2	CG	HG1	HG2	CE	ME
M11	115.0	7.80	54.5	4.65	32.1	2.04	2.04	33.2	2.50	2.31		
M85	122.3	9.37	54.8	5.01	39.6	2.21	1.89	32.3	2.46	2.26	37.4	1.51
M113	123.8	8.60	53.9	5.44	38.0	1.98	1.64	30.2	2.46	2.32	35.1	2.18
M130	120.4	7.57	56.9	4.72	31.2	2.18	2.18	31.9	2.63	2.28		

PHE	N	HN	CA	HA	CB	HB1	HB2	CD	HD	CE	HE	CZ	HZ
F39	125.9	9.84	57.3	4.18	37.7	2.97	2.86	129.2	6.67	130.6	6.86	128.4	6.93
F58	118.7	7.86	58.8	3.97	37.7	2.95	2.74	130.3	6.72	131.4	7.01	132.9	7.21
F83	114.0	8.02	57.5	4.88	37.7	3.60	3.38		7.33		7.02		
F98	119.7	8.35	55.5	4.90	41.8	3.43	2.65		7.08	130.6	7.22		7.31

PRO	N	HN	CA	HA	CB	HB1	HB2	CG	HG1	HG2	CD	HD1	HD2
P28			63.2	4.52	32.7	2.13	1.62	27.8	1.98	1.81	50.3	3.77	3.73
P35			63.4	4.24	31.1	2.28	1.88	27.7	2.11	2.02	51.2	4.14	3.77
P44			65.7	3.92	32.3	2.23	1.96		1.09	1.82			
P96			63.2	4.25	32.5	2.00	1.33	27.5	1.92	1.92	50.3	3.75	3.54

SER	N	HN	CA	HA	CB	HB1	HB2
S27	118.7	8.10	55.4	4.68	63.1	3.89	3.74
S29	114.2	7.96	57.5	4.51	65.5	3.97	3.82
S56	114.4	8.29	60.1	4.53	64.3	3.84	3.84
S57	122.0	8.86	61.7	4.31	64.0	3.92	3.82
S71	118.5	9.51	57.1	4.86	65.0	3.75	3.63
S76	124.4	8.21	56.5	4.92	64.3	4.07	3.83
S84	110.8	7.04	57.3	5.78	68.2	3.73	3.66
S91	120.1	8.44	56.7	4.63	65.4	3.72	3.53
S132	113.7	8.38	61.7	3.98	63.6	3.83	3.83
S137	115.4	7.50	58.1	4.57	63.8	4.14	4.01

THR	N	HN	CA	HA	CB	HB	CG	MG
T15	111.1	8.00	64.0	4.28	71.1	4.29	22.1	1.17
T38	120.1	8.28	65.1	4.33	70.1	3.62	23.2	1.03
T43	119.5	8.36	58.9	4.89	69.7	4.66	22.4	1.24
T64	111.1	8.30	59.9	5.30	72.0	3.50	21.5	0.91
T89	117.2	9.19	63.4	4.69	69.7	4.50	23.4	1.43
T92	115.8	8.28	61.5	4.59	70.6	4.16	21.6	1.16
T97	111.5	7.69	59.7	3.67	71.5	4.11	21.9	1.00
T101	123.0	8.45	63.1	5.62	73.8	3.54	23.6	1.43
T103	120.5	9.25	60.3	5.39	72.0	3.88	22.9	1.15
T105	121.0	9.63	60.8	4.51	67.5	4.79	22.5	1.02
T108	112.7	7.77	60.0	5.27	72.1	3.27	21.5	0.25

TRP	N	HN	CA	HA	CB	HB1	HB2	CD1	HD1	NE1	HE1	CZ2	HZ2	CH2	HH2	CE3	HE3	Z3	HZ3
W3	122.0	8.00	59.1	4.59	30.2	3.42	3.02		7.34	129.7	9.56	119.2	7.52	121.2	6.61	115.1	6.8 1	123.7	5.98
W31	107.2	9.07	57.0	4.76	28.4	2.46	2.46	124.4	6.81	127.4	10.00		7.32	123.2	6.97		5.25	122.0	6.21

TYR	N	HN	CA	HA	CB	HB1	HB2	CD	HD	CE	HE
Y6	117.0	7.28	60.9	4.28	37.7	3.22	3.22	132.5	7.33	117.9	6.56
Y24	116.4	6.73	56.0	4.72	40.6	2.97	2.05	133.1	6.60	118.0	6.70
Y59	121.6	8.05	61.6	4.46	37.7	3.26	3.04	132.9	7.39	118.5	6.96
Y128	121.6	9.13	62.0	4.04	38.7	3.18	3.18	133.2	7.07	118.2	6.88
Y139	124.9	8.12	59.9	4.45	41.5	2.63	2.63	132.9	7.21	117.9	6.98

Table I (Continued)

VAL	N	HN	CA	HA	CB	HB	CG1	MG1	CG2	MG2
V22	129.3	9.10	60.1	4.09	36.5	1.60	22.6	0.59	20.7	0.47
V30	123.6	8.91	64.2	3.75	32.1	2.17	22.5	0.95	23.0	0.80
V34	123.5	7.49	61.2	4.24	32.4	2.35	23.4	1.29	21.3	1.00
V40	120.3	9.75	63.5	3.64	31.2	2.02	22.0	0.99	19.4	0.75
V47	121.6	8.03	67.7	3.23	31.0	2.06	21.8	0.83	24.0	0.76
V49	120.9	7.33	66.0	3.73	32.1	2.09	22.6	1.08	22.1	1.08
V51	132.5	7.55	60.8	4.32	31.2	2.25	18.1	0.79	21.6	0.24
V60	118.3	7.58	64.0	4.05	33.0	2.06	21.5	0.98	21.2	0.98
V72	125.3	9.09	63.5	3.76	32.1	1.58	21.5	0.44	21.4	0.28
V100	123.6	8.59	59.5	5.56	37.5	1.79	23.0	1.05	21.5	0.88
V102	127.8	9.08	59.7	5.15	35.0	1.76	22.4	0.74	21.5	0.67
V110	123.5	8.73	61.2	4.53	32.2	2.00	22.0	0.82	21.9	0.64
V118	122.4	7.44	63.7	4.01	32.1	2.08	18.1	1.19	22.1	1.11

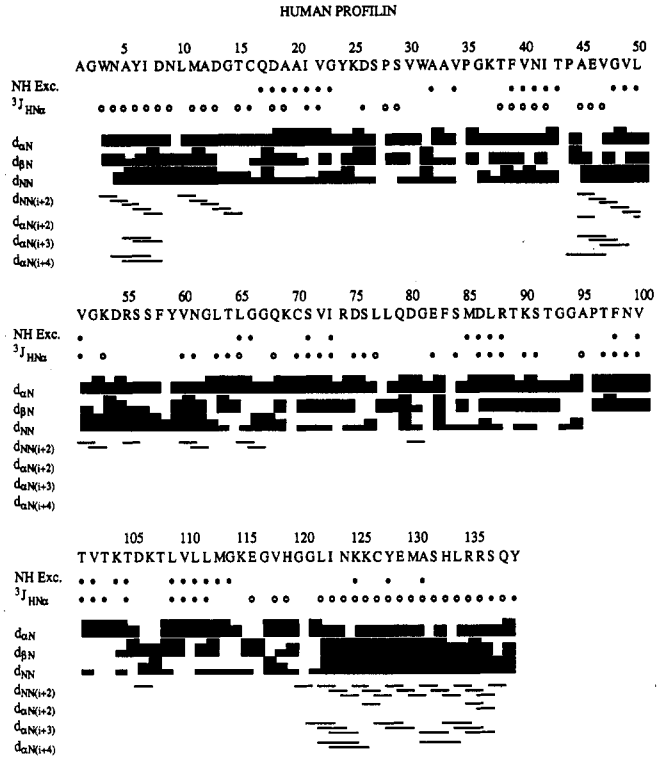

FIGURE 3: Summary of the sequential and short-range NOEs observed for human profilin. Symbols: (●) residues with slowly exchanging amide hydrogens or with a large (>8.0 Hz) value for $^3J_{HN\alpha}$; (○) residues with a small (<5.0 Hz) for $^3J_{HN\alpha}$. For the sequential NOEs, the relative intensity of the NOE is represented by the thickness of the bar.

amide protons. Evidence for helical structure is also observed for residues 45–51. These residues have strong sequential NN NOEs, as well as NN(i,i+2) and several αN(i+3) NOEs, and small coupling constants. In addition, residues 47–50 have reduced exchange rates with the solvent. Residues 37–41 also have small values for $^3J_{HN\alpha}$ coupling constants, and residues 38–42 have slowing exchanging amide hydrogens, suggesting a helical conformation in this region; however, corroborating NOEs, aside from strong sequential NN NOEs, were not detected.

Long-range NOEs were identified that define proton–proton interactions between adjacent strands of a β-sheet. The pattern of cross-strand Hα–Hα, Hα–HN, and HN–HN NOEs indicated that the strands of the β-sheet are antiparallel to each other; these NOEs are illustrated in Figure 4. Also shown in Figure 4 are the amide hydrogens that have reduced exchange rates with solvent. As can be seen in the figure, human profilin contains a seven-stranded, antiparallel β-sheet. Five strands, defined as C–G and spanning residues 63–114, are contiguous in sequence and are in an "up-down" motif. The remaining two β-strands, A and B, span residues 18–35; these two β-strands adjoin the remaining five β-strands through interactions between residues 108–114 and residues 18–24. Two tight turns connect the β-strands C–D and F–G. The second of these turns is characterized by large NN and NN(i,i+2) NOEs and a large value for $^3J_{HN\alpha}$, suggestive of a type I turn (Lewis et al., 1973). The loops between the remaining β-strands could not yet be classified; it is likely that these regions possess a significant amount of irregular structure and/or are mobile in solution.

Correlation of Cα and Cβ Chemical Shifts with Secondary Structure. Recently, correlations have been observed between the Cα (Spera & Bax, 1991; Wishart et al., 1991; Fairbrother et al., 1992) and Cβ (Spera & Bax, 1991) chemical shifts and the local backbone conformation for a number of proteins with known structures. Relative to random coil chemical shifts, Cα resonances tend to shift upfield in β-sheets and extended strands, and they tend to shift downfield in helices. The opposite trend holds for the Cβ resonances. Figure 5 panels A and B present the secondary shifts, i.e., the deviations between observed and random coil chemical shift values, for the Cα and Cβ resonances of profilin. Because the Cα and Cβ secondary shifts are of similar magnitude and opposite sign for both helices and sheets, subtraction of the Cα and Cβ secondary shifts enhances the correlation between the secondary structural elements and the secondary shifts. Figure 5C shows the result of such a subtraction. Figure 5D presents the same data in Figure 5C after applying a three-point smoothing function to the data. Although local and regional details of the secondary structural elements of profilin can be extracted from the plots of Figure 5A,B, the smoothed and enhanced secondary shifts in Figure 5D highlight the regions of secondary structure more clearly. Examination of this latter plot indicates the presence of four potentially helical regions, from residues 3–14, 45–50, 57–60, and 122–139. The N- and C-terminal helices and helix 46–51 are in agreement with the analysis of the short-range structural data. For the potential helical region from residues 58–61, the NOE data are more consistent with a series of turns or, possibly, a transiently stable helix. β-Strand secondary structure is predicted for residues 17–23, 32–34, 63–65, 68–76, 84–92, 97–104, and 107–113. The regions of β-strands correspond very well with the NOE, $^3J_{HN\alpha}$ coupling constant, and amide hydrogen exchange data discussed above.

Structure Determination of Human Profilin. Restraints for the structure determination were derived from the ^{15}N-edited and ^{13}C-edited spectra as described under Experimental Procedures. The goal of the structure determination was to obtain second generation structures (Clore & Gronenborn, 1991) that would accurately describe the three-dimensional folding pattern of human profilin. The calculated structures

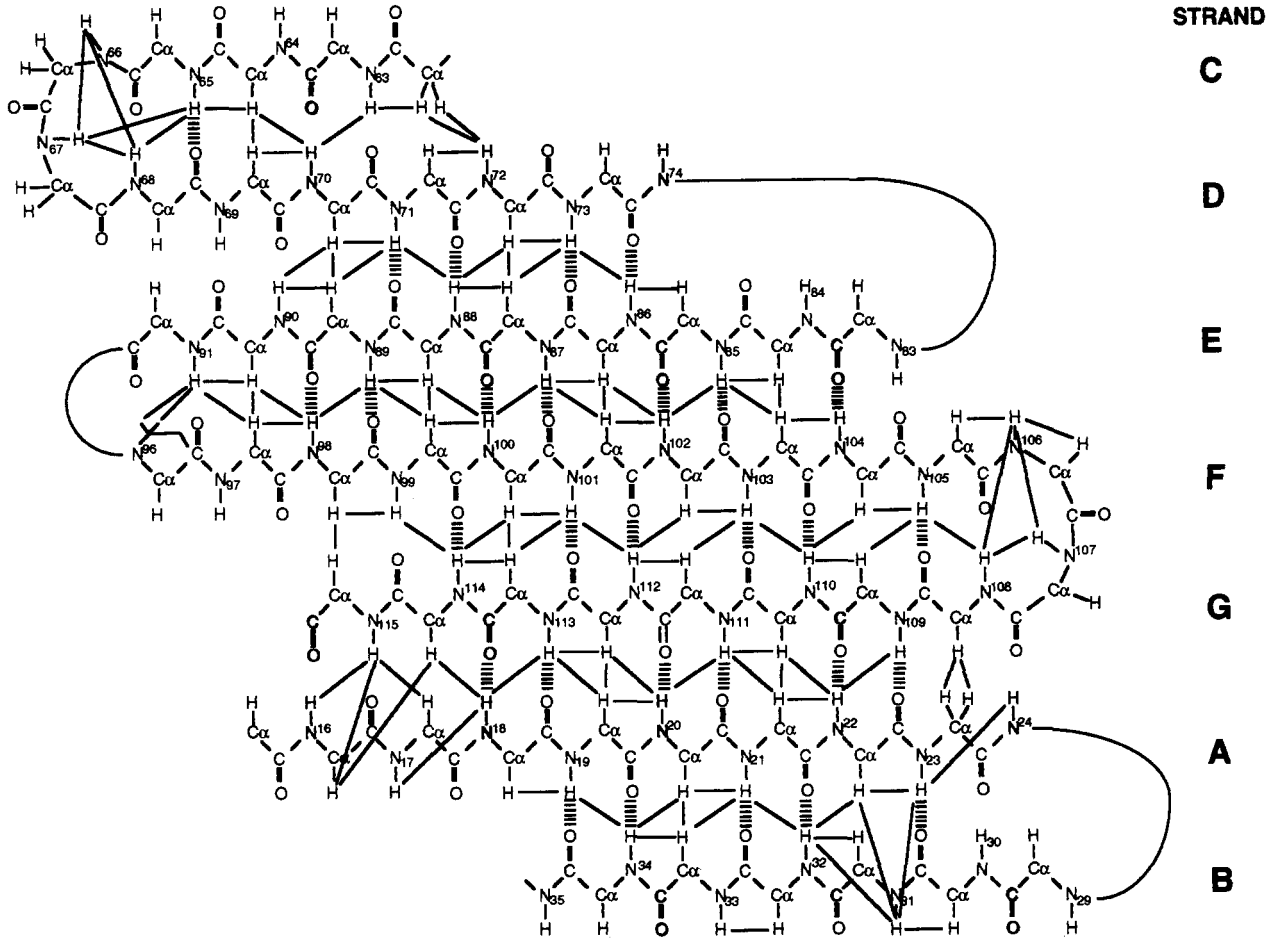

FIGURE 4: Short sequential and long-range backbone NOEs observed for the β-sheet region of human profilin. NOEs are indicated by bars, and slowly exchanging amide hydrogens are in bold. Hatched bars indicate hydrogen bonds included in the structure determination. Strands of the β-sheet are classified in sequential order from the N-terminus and are referenced by letters A–G.

converged well; superposition of the backbone atoms (N, Cα, C, O) gave an average rmsd of 1.5 Å to the average structure for all residues and an average rmsd of 1.2 Å for those residues involved in secondary structure. Figure 7 shows a schematic representation of the profilin backbone. The current NMR structures contain several distance restraint violations greater than 1.0 Å, with the largest single violation being 1.45 Å. These NOE violations are not expected to alter the global folding pattern reported here.

Profilin is an α/β protein. Using backbone Φ and Ψ torsion angles as the criterion for secondary structure, the following residues comprise the sheets and helices of profilin: helix A, 4–13; helix B, 44–51; helix C, 122–137; strand A, 18–22; strand B, 32–34; strand C, 63–65; strand D, 68–73; strand E, 84–91; strand F, 97–105; and strand G, 108–115. Residues 105–108 form a type I turn.

The core of the protein is comprised of a seven-stranded antiparallel β-sheet that folds into an incomplete β-barrel. Using the nomenclature of Richardson (1981) for describing β-sheet topology, profilin's sheet topology is +1, −6x, +1, +1, +1, +1. The strands show the distinct right-handed twist that is commonly observed in β-sheets. The type I turn connects strands F and G of the sheet; the remaining turns are less precisely defined in the current structures.

Two extended α-helices emanate from the N- and C-terminal strands of the sheet (strands A and G). These helices (A and C) lie adjacent to one another on one side of the β-sheet, in an orientation that is roughly parallel to the strands of the sheet. The two helices are antiparallel to each other. Helices A and C show distinct curvature of their helix axes, tending to follow the twist in the β-sheet. Such curvature has been observed previously in other proteins and has been attributed to hydrogen bond effects (Barlow & Thornton, 1988). Both helices are strongly amphipathic, and the curvature of the helix axes facilitates optimal hydrophobic interactions at the interface of the helices and sheet. These hydrophobic interactions occur predominantly between helix C and strands F and G, and between helix A and strands A and B.

On the opposite face of the sheet lies a third helix. This helix is situated such that it interacts with the ends of strands F, G, A, and B of the β-sheet with a helix axis that is roughly perpendicular to the axes of the N- and C-terminal helices. This helix makes up part of the crossover loop that connects strands B and C of the β-sheet. The remainder of this crossover loop has less regular secondary structure. Residues 38–41 form a structure characteristic of one turn of a 3–10 helix or type III turn (Lewis et al., 1977); however, the structures will need to be refined further before this can be fully ascertained.

DISCUSSION

The purification procedure used in obtaining sufficient quantities of human profilin for study by NMR subjected the protein to atypical environmental conditions. Recovering profilin from the poly(L-proline) column required elution in 6 M urea followed by renaturation. To ascertain the biological integrity of profilin, we examined its binding to actin, PIP_2, and poly(L-proline). The binding was similar to that observed with bovine profilin isolated from calf spleen, indicating that the profilin was indeed functional (T. B. Lavoie, unpublished).

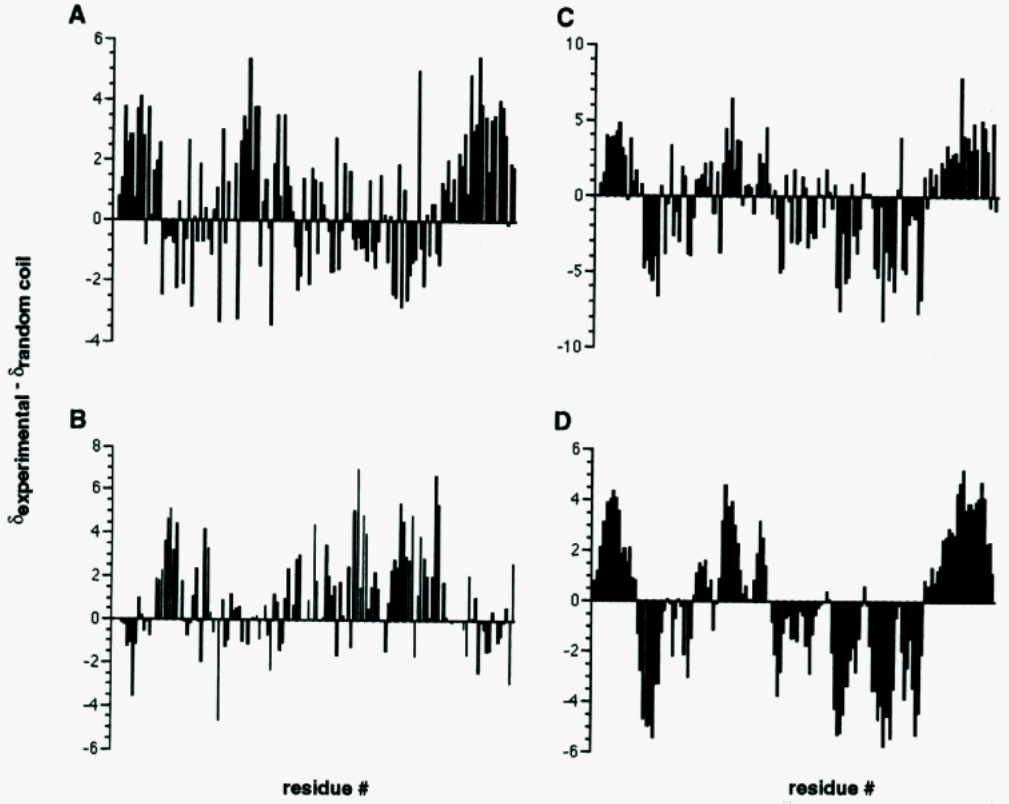

FIGURE 5: Histogram showing the observed secondary shifts, defined here as the measured ^{13}C chemical shift minus the "random coil" ^{13}C chemical shift (Spera & Bax, 1991), for the (A) Cα and (B) Cβ chemical shifts of profilin. The correlations between secondary structure and the secondary shifts are enhanced by subtracting the $^{13}C\beta$ secondary shifts from the $^{13}C\alpha$ secondary shifts (C), followed by application of a three-point smoothing function to the data (D). Helical and extended regions are observed as positive and negative peaks, respectively, in panels C and D.

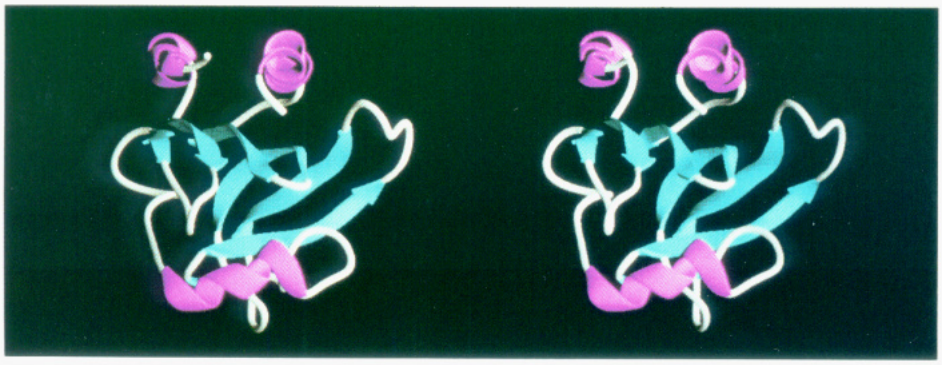

FIGURE 6: Schematic stereoview of one structure of the human profilin ensemble. The β-strands are represented by flat ribbons with arrows indicating the chain direction. Helices are represented by curled ribbons. The drawing was generated with the program RIBBONS (Carson, 1991).

```
                1                   20                  40                  60
Human     AGWNAYID-NLMADGTCQDAAIVGYKDSPSVWAAVPGKTFVNITPAEVGVLVGKDRSSFYV--NGLTLGG
Acanth.   -SWQTYVDTNLVGTGAVTQAAILGL--DGNTWATSAG---FAVTPAQGQTLASAFNNADPIRASGFDLAG

                   80                  100                 120                 139
Human     QKCSVIRDSLLQDGEFSMDLRTKSTGGAPTFNVTVTKTDKTLVLLMGKEGVHGGLINKKCYEMASHLRRSQY
Acanth.   VHYVTLRAD-----DRSIYGKK------GSAGVITVKTSKSILVGVYNEKIQPGTAANVVEKLADYLIGQGF
```

FIGURE 7: Amino acid sequence alignment of human profilin (Kwiatkowski & Bruns, 1988) and *Acanthamoeba* profilin I (Ampe et al., 1985). In aligning the sequences, the conserved secondary structural elements between the two proteins were optimized and gaps resulting from deletions were constrained to contiguous segments when possible. Corresponding helices and β-strands are shaded in lighter and darker gray, respectively. The secondary structures are those experimentally determined by NMR: human profilin (this report) and *Acanthamoeba* profilin (Archer et al., 1993).

The assignment of the ^1H, ^{15}N, and ^{13}C resonances of profilin was achieved by a combination of several recently developed triple-resonance NMR techniques. Assignment of these resonances is the crucial first step toward determination of the three-dimensional structure of profilin. In addition, the assignments provide numerous atomic probes that can be exploited in studies aimed at understanding the interaction of profilin with other macromolecules and ligands. For example,

by monitoring changes in chemical shifts of the backbone ^1H and ^{15}N resonances of profilin upon complex formation, we have identified the region of profilin involved in binding poly(L-proline) to be at the interface between the N- and C-terminal helices and the β-sheet (Metzler et al., 1994).

Three-dimensional ^{15}N- and ^{13}C-edited NOESY-HMQC spectra afforded numerous distance restraints enabling the three-dimensional structure of human profilin to be determined. Many NOE cross-peaks remained unassigned due to spectral overlap, but, as can be seen by the results presented here, these spectra were more than sufficient to allow convergence of the profilin structure. The structure of profilin at its current level of refinement corresponds to a second generation structure, having on average nine restraints per residue with a backbone rmsd of 1.5 Å (Clore & Gronenborn, 1991). Higher resolution structures will require analysis of four-dimensional NOE spectra and additional analysis of the three-dimensional NOE spectra to increase the density of restraints per residue. Stereospecific assignments and side chain dihedral angle constraints will also increase the resolution of the structure. This analysis is currently underway.

Evidence for the secondary structural elements of profilin came from assignment of the NOE cross-peaks, measurement of the $^3J_{HN\alpha}$ coupling constants and amide hydrogen exchange rates, and the deviation of Cα and Cβ chemical shift from their respective shifts when in a random coil conformation. These secondary structural features were consistent with the calculated three-dimensional structures of profilin.

Amino acid preferences have been empirically determined for specific locations at the ends of α-helices (Richardson & Richardson, 1988). Examination of the amino acid positioning in the three helices of profilin indicates that they all fall into typical classifications. Helix A spans Asn 4–Gly 14. Asparagine occurs preferentially at position 1 of a helix, often serving as an N-cap residue where its side chain CO group can form a hydrogen bond to backbone NH of a residue one turn C-terminal to it. Helix A terminates with glycine, a residue prevalent at the C-cap position. Similar trends are seen for helix B, which spans residues 44–51. Helix B begins with proline 44. Prolines have been described as helix initiators because they are often found at position 1 of a helix. N-terminal to Pro 44 is Thr 43, a residue commonly found at the N-cap position. Thr 43 has the standard conformation of an N-cap residue ($\phi \sim 85$, $\psi \sim 175$) (Richardson & Richardson, 1988) which positions its side chain hydroxyl group in a position favorable for making a hydrogen bond with the NH of Glu 46. As seen with helix A, helix B is terminated with a glycine residue (Gly 52). Helix C is bounded by Gly 121 and Gln 138, residues that show a strong preference for these positions.

Several of the amide hydrogens exhibit very weak ^1H–^{15}N HSQC cross-peaks. These hydrogens include G81, T92, G94, and G121. Each of these residues occurs in a turn, either connecting two β-strands or, in the case of G121, between β-strand G and helix C. All of these amide hydrogens are completely exposed to solvent. The dynamic properties that contribute to the reduced HSQC cross-peak intensities for these residues remain to be determined. Studies of the backbone dynamics of profilin by ^{15}N relaxation measurements are in progress.

The secondary structure of profilin I from *Acanthamoeba* has been reported (Archer et al., 1993). Comparison of the secondary structure of *Acanthamoeba* profilin with that determined here for human profilin shows that the two proteins are quite similar (Figure 7). All helices and β-strands can be easily aligned, suggesting that the three-dimensional structure of *Acanthamoeba* profilin I should be similar to that of the human analogue.

The similarity between the structures of human and *Acanthamoeba* profilin is not unexpected since the sequences of the two proteins are approximately 30% homologous. However, low sequence homology in the C-terminal half of the molecules had led to several different potential alignments of the amino acid sequences (Takagi et al., 1990; Binette et al., 1990; Kwiatkowski & Bruns, 1988; Pollard & Rim, 1991). Sequence alignment based on the experimentally determined secondary structures of *Acanthamoeba* profilin (Archer et al., 1993) and human profilin (this report) facilitate this sequence alignment (Figure 7). Three of the four deletions in *Acanthamoeba* profilin, residues 25–26, 77–81, and 90–95 in the human profilin sequence, involve loop regions connecting two contiguous β-strands of the sheet and thus are easily accommodated by the structure. The deletion 90–95 reduces the β-sheet by one amino acid on each side of the loop. The fourth deletion, residues 37–39, occurs in a coiled section of the protein between strand B and helix B. It too can be easily accommodated with little disruption of the overall profilin fold.

The sequence alignment presented in Figure 7 is very similar to that proposed of Binette et al. (1990) and Pollard and Rimm (1991). However, a significant difference exists in the alignment 79–99, particularly in the MDLR stretch. In previous alignments, the human profilin residues MDLR are suggested to make up one of the three stretches of amino acids in this region that are deleted in the lower eukaryotic sequences. These residues comprise the center residues of strand E of the β-sheet in human profilin. It is unlikely that these residues are deleted, especially since this strand of sheet is conserved in the *Acanthamoeba* profilin structure. The modified sequence alignment presented here has just two deletions in this region; this alignment not only is more consistent with the newly acquired structural information on profilins but is also a more direct solution to the alignment problem because it minimizes the number of gaps in the alignment. The most interesting feature of this modified sequence alignment is that Arg 88, which was previously considered to be deleted and thus unimportant, is now in the position of a conserved positive charge. Conserved positive charges are believed to be important for PIP_2 binding (see below).

Helix A in the human profilin structure is substantially longer than that found by NMR secondary structure analysis of *Acanthamoeba* profilin. There is one insertion in the *Acanthamoeba* profilin sequence with respect to the human profilin sequence. This insertion places a threonine between residues 8 and 9 in helix A. Although threonines have no statistical preference either for or against helices, the insertion of threonine in the helix could possibly cause a 100° rotation and a 1.5-Å translation of the helical residues C-terminal or N-terminal to it, resulting in the loss of stabilizing hydrophobic interactions of helix A with helix C and the β-sheet. This may explain why the helix A in *Acanthamoeba* profilin is shorter than that observed in human profilin.

Cross-linking studies between *Acanthamoeba* profilin and actin have implicated Lys 115 of *Acanthamoeba* profilin as an important residue for formation of the profilin–actin complex (Vandekerckhove et al., 1989). Moreover, the residues surrounding Lys 115 have been found to be similar to the sequences from other actin-binding proteins (Ampe & Vandekerckhove, 1987), leading to the suggestion that these residues comprise part of an ancient actin-binding site. Recent

binding studies have shown that a peptide homologous to this region of profilin can bind to actin (den Hartigh et al., 1992), supporting the importance of these residues in actin binding. These residues are located in the C-terminal helix, leading to the suggestion that part of the ancient actin-binding domain is a long α-helix. Lys 115 of *Acanthamoeba* profilin corresponds to Glu acid 129 in human profilin. In addition to Glu acid 129, there are numerous charged residues on this face of helix C, including Lys 125, Lys 126, Arg 135, Arg 136, and possibly His 133. Thus, the interaction of profilin with actin may have a large electrostatic component; the details of this interaction should become apparent upon completion of the X-ray crystallographic analysis of the complex by Schutt and co-workers (Schutt et al., 1993).

Profilin also binds the membrane phospholipid phosphatidylinositol 4,5-bisphosphate (PIP_2). The binding of PIP_2 inhibits the interaction of profilin with actin and can thereby regulate the cellular process of cytoskeleton rearrangement. The phosphate groups of PIP_2 appear to be important for the interaction of PIP_2 with profilin, implicating the basic amino acids of profilin. The basic residues located in the C-terminal helix of profilin described above provide a suitable positive patch by which PIP_2 can both bind to human profilin and directly inhibit the interaction between profilin and actin. Other regions of profilin have also been proposed as being important for PIP_2 binding. Examination of the conservation of positively charged amino acids, taken together with the affinity of different profilins for PIP_2 (Machesky et al., 1989), has led to the suggestion that Lys 66 of *Acanthamoeba* profilin may be important for PIP_2 binding (Haarer & Brown, 1990). This residue is also conserved in human profilin as Lys 69. Lys 69 lies on the opposite side of the profilin molecule from the proposed actin-binding site, suggesting that PIP_2 may interfere with actin binding in an allosteric manner. Since PIP_2 binds profilin with a stoichiometry of about five PIP_2s per profilin (Machesky et al., 1989), other residues clearly must be involved. The mechanism for PIP_2 binding may become apparent when these residues are identified.

The intense interest in profilin has resulted in the initiation of projects aimed at its structural characterization by several groups. *Acanthamoeba* profilin I is under investigation by both NMR (Archer et al., 1993) and crystallographic methods (Magnus et al., 1988). In addition, crystallographic analysis of bovine profilactin (Schutt et al., 1989, 1993) will provide a structure of profilin when bound to actin. It will be interesting to compare the structures of profilin from various species and in free and actin-bound forms when they become available. More importantly, the structure of profilin presented here provides a framework upon which the correlations between structure and function can begin to be explored.

ACKNOWLEDGMENT

We gratefully thank David Kwiatkowski for providing the cDNA clone of human profilin, Gary Babcock for providing the vector used in subcloning the human profilin gene, and Kevin Leong for preparation of the poly(L-proline) column. We also thank Vidya Raghunathan for sharing her experiences with profilin and for providing a copy of her Ph.D. thesis. We are indebted to Clarence Schutt for stimulating interest in profilin.

REFERENCES

Ampe, C., & Vandekerckhove, J. (1987) *EMBO 6*, 4149–4157.

Ampe, C., Vandekerckhove, J., Prenner, S. L., Tobacman, L., & Korn, E. D. (1985) *J. Biol. Chem. 260*, 834–840.

Archer, S. J., Vinson, V. K., Pollard, T. D., & Torchia, D. A. (1993) *Biochemistry 32*, 6680–6687.

Barlow, D. J., & Thornton, J. M. (1988) *J. Mol. Biol. 201*, 601–619.

Bax, A., Clore, G. M., Driscoll, P. C., Gronenborn, A. M., Ikura, M., & Kay, L. E. (1990) *J. Magn. Reson. 87*, 620–627.

Billeter, M., Neri, D., Otting, G., Qian, Y. Q., & Wüthrich, K. (1992) *J. Biomol. NMR 2*, 257–274.

Binette, F., Benard, M., Laroche, A., Pierron, G., Lemieux, G., & Pallotta, D. (1990) *DNA Cell Biol. 9*, 323–334.

Bodenhausen, G., & Ruben, D. J. (1980) *Chem. Phys. Lett 69*, 185–188.

Brunger, A. T. (1992) X-PLOR version 3.1, Yale University Press, New Haven, CT.

Carson, M. (1991) *J. Appl. Crystallogr. 24*, 958–961.

Clore, G. M., & Gronenborn, A. M. (1991) *Science 253*, 1390–1399.

Clore, G. M., Bax, A., Driscoll, P. C., Wingfield, P. T., & Gronenborn, A. M. (1990) *Biochemistry 29*, 8172–8184.

Constantine, K. L., Madrid, M., Banyai, L., Trexler, M., Patthy, L., & Llinas, M. (1992) *J. Mol. Biol. 223*, 239–256.

Constantine, K. L., Goldfarb, V., Wittekind, M. Friedrichs, M. S., Anthony, J., Ng, S.-C., & Mueller (1993) *J. Biomol. NMR 3*, 41–54.

den Hartigh, J. C., van Bergen en Henegouwen, P. M. P., Verkleij, A. J., & Boonstra, J. (1992) *J. Cell. Biol. 119*, 349–355.

Fairbrother, W. J., Palmer, A. G., Rance, M., Reizer, J., Saier, M. H., Jr., & Wright, P. E. (1992) *Biochemistry 31*, 4413–4425.

Goldschmidt-Clermont, P. J., & Janmey, P. A. (1991) *Cell 66*, 419–421.

Goldschmidt-Clermont, P. J, Machesky, L. M., Baldassare, J. J., & Pollard, T. D. (1990) *Science 247*, 1575–1578.

Goldschmidt-Clermont, P. J., Kim, J. K., Machesky, L. M., Ree, S. G., & Pollard, T. D. (1991a) *Science 251*, 1231–1233.

Goldschmidt-Clermont, P. J, Machesky, L. M., Doberstein, S. K., & Pollard, T. D. (1991b) *J. Cell Biol. 113*, 1081–1089.

Grzesiek, S., & Bax, A. (1992) *J. Am. Chem. Soc. 114*, 291.

Haarer, B. K., & Brown, S. S. (1990) *Cell Motil. Cytoskeleton 17*, 71–74.

Ikura, M., Kay, L. E., Tschudin, R., & Bax, A. (1990) *J. Magn. Reson. 86*, 204–209.

Lassing, I., & Lindberg, U. (1985) *Nature 314*, 472–474.

Lewis, P. N., Momany, F. A., & Scheraga, H. A. (1977) *Biochim. Biophys. Acta. 303*, 211–229.

Kaiser, D. A., Goldschmidt-Clermont, P. J., Levine, B. A., & Pollard, T. D. (1989) *Cell Motil. Cytoskeleton 14*, 251–262.

Kay, L. E., & Bax, A. (1989) *J. Magn. Reson. 86*, 110–126.

Kay, L. E., Wittekind, M., McCoy, M. A., Friedrichs, M. S., & Mueller, L. (1992) *J. Magn. Reson 98*, 443–452.

Kwiatkowski, D. J., & Bruns, G. A. P. (1988) *J. Biol. Chem. 263*, 5910–5915.

Machesky, L. M., Goldschmidt-Clermont, P. J., & Pollard, T. D. (1989) *J. Cell Biol. 109*, 268a.

Magnus, K. A., Lattman, E. E., Kaiser, D. A., & Pollard, T. D. (1988) *Biophys. J. 53*, 28a.

Marion, D., Driscoll, P. C., Kay, L. E., Wingfield, P. T., Bax, A., Gronenborn, A. M., & Clore, G. M. (1989a) *Biochemistry 28*, 6150–6156.

Marion, D., Kay, L. E., Sparks, S. W., Torchia, D. A., & Bax, A. (1989b) *J. Am. Chem. Soc. 111*, 1515–1517.

Metzler, W. J., Valentine, K., Roebber, M., Friedrichs, M. S., Marsh, D. G., & Mueller, L. (1992) *Biochemistry 31*, 5117–5127.

Metzler, W. J., Bell, A. J., Ernst, E. G., Lavoie, T. B., & Luciano Mueller, (1994) *J. Biol. Chem.* (in press).

McCoy, M. A., & Mueller, L. (1992) *J. Am. Chem. Soc. 113*, 2108.

Mockrin, S. C., & Korn, E. D. (1980) *Biochemistry 19*, 5359–5362.

Mueller, L., & Ernst, R. R. (1978) *Mol. Phys. 38*, 963–992.
Mueller, L., Campbell-Burk, S., & Domaille, P. (1992) *J. Magn. Reson. 96*, 408–415.
Nilges, M., Gronenborn, A. M., & Clore, G. M. (1988) *FEBS Lett. 239*, 129–136.
Olejniczak, E. T., Xu, R. X., Petros, A. M., & Fesik, S. W. (1992) *J. Magn. Reson. 100*, 444.
Pollard, T. D., & Rimm, D. L. (1991) *Cell Motil. Cytoskeleton 20*, 169–177.
Richardson, J. S. (1981) *Adv. in Protein Chem. 34*, 167–337.
Richardson, J. S., & Richardson, D. C. (1988) *Science 240*, 1648–1652.
Schutt, C. E., Lindberg, U., Myslik, J., & Strauss, N. (1989) *J. Mol. Biol. 209*, 735–746.
Schutt, C. E., et al. (1993) *Nature* (submitted).
Shaka, A. J., Lee, C. J., & Pines, A. (1988) *J. Magn. Reson. 77*, 274–293.
Spera, S., & Bax, A. (1991) *J. Am. Chem. Soc. 113*, 5490–5492.
States, D. J., Haberkorn, R. A., & Ruben, D. J. (1982) *J. Magn. Reson. 48*, 286–292.
Takagi, T., Mabuchi, I., Hosoya, H., Furuhashi, K., & Hatano, S. (1990) *Eur. J. Biochem. 192*, 777–781.
Vandekerckhove, J. S., Kaiser, D. A., & Pollard, T. D. (1989) *J. Cell Biol. 109*, 619–626.
Wishart, D. S., Sykes, B. D., & Richards, F. M. (1991) *J. Mol. Biol. 222*, 311–333.
Wittekind, M., & Mueller, L. (1993) *J. Magn. Reson. Ser. B 101*, 201–205.
Wittekind, M., Metzler, W. J., & Mueller, L. (1993) *J. Magn. Reson. Ser. B 101*, 214–217.
Zhu, G., & Bax, A. (1990) *J. Magn. Reson. 90*, 405–410.
Zuiderwig, E. R. P., & Pesik, S. W. (1990) *Biochemistry 28*, 2387–2391.
Zuiderweg, E. R. P., Mc Intosh, L. P., Dahlquist, F. W., & Fesik, S. W. (1990) *J. Magn. Reson. 86*, 210–216.